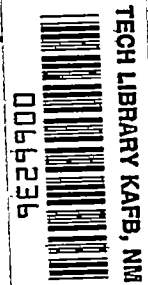# NATIONAL ADVISORY COMMITTEE FOR AERONAUTICS

TECHNICAL NOTE 3287

HEAT TRANSFER FROM A HEMISPHERE-CYLINDER

EQUIPPED WITH FLOW-SEPARATION SPIKES

By Jackson R. Stalder and Helmer V. Nielsen

Ames Aeronautical Laboratory
Moffett Field, Calif.

NACA

Washington

September 1954

NATIONAL ADVISORY COMMITTEE FOR AERONAUTI(

TECHNICAL NOTE 3287

HEAT TRANSFER FROM A HEMISPHERE-CYLINDER

EQUIPPED WITH FLOW-SEPARATION SPIKES

By Jackson R. Stalder and Helmer V. Nielsen

SUMMARY

Tests were conducted to determine the effects on average heat transfer, average recovery temperature, and pressure distribution caused by attaching spikes to the front of a hemispherical-nosed body of revolution. The investigation was concerned primarily with a series of conical-nosed spikes of semiapex angle 10° and length to body-diameter ratio 0.5 to 2.0. In addition, the effect on heat transfer of capping the spikes with flat disks and blunt cones of semiapex angle 40° was also investigated at a Mach number of 2.67 and a Reynolds number of 2.85×10^5.

The range of investigation was from Reynolds number 1.55 to 9.85×10^5 (based on body diameter) and from Mach number 0.12 to 5.04.

Although the tests confirmed previous results which showed a reduction of drag on attaching spikes to a hemispherical nose at supersonic speeds, it was found that the rate of heat transfer is approximately doubled regardless of spike length or configuration. It was also found that this increase in heat transfer is confined almost entirely to the forward half-area of the hemisphere. Average temperature-recovery factors are lowered slightly on the addition of spikes, decreasing with increasing spike length. At a Mach number of 1.75 the 2-inch spike reduced the recovery factor by 3 to 5 percent, depending on the Reynolds number; at a Mach number of 2.67 the reduction was from 5 to 10 percent.

For the hemisphere without spikes it was found that the Nusselt numbers measured at subsonic and supersonic airspeeds could be correlated as a function of Reynolds number alone, provided the air properties were evaluated behind the normal shock waves. Thus, it is possible to predict supersonic heat transfer from a hemisphere by using subsonic data.

INTRODUCTION

Interest has been expressed in the use of spikes protruding in front of blunt bodies as a means of reducing their drag. Mair (ref. 1) and Moeckel (ref. 2) examined, in some detail, the mechanism of flow separation ahead of two-dimensional and axially symmetric bodies equipped with various length spikes and found appreciable drag reductions at supersonic speeds.

In view of the drag reductions resulting from the use of spikes, it was apparent that information was needed concerning the effect of spikes on heat transfer to blunt-nosed bodies. Consequently, the present investigation was undertaken to measure the heat-transfer and recovery-temperature characteristics of a hemispherical-nosed cylinder with and without drag-reduction spikes over a range of Mach numbers and Reynolds numbers.

NOTATION

A surface area of hemispherical nose, sq ft

C_D pressure drag coefficient, dimensionless

C_P pressure coefficient, dimensionless

D drag, lb

d diameter, ft

h average heat-transfer coefficient, BTU/sec, sq ft, $^\circ$F

k thermal conductivity, BTU/sec, sq ft, $^\circ$F/ft

l spike length, ft

M Mach number, dimensionless

Nu Nusselt number, $\dfrac{hd}{k}$, dimensionless

P pressure, lb/sq ft

Q heat rate, BTU/sec

Re Reynolds number, $\dfrac{v\rho d}{\mu}$, dimensionless

r   temperature-recovery factor, $\dfrac{T_r - T_\infty}{T_0 - T_\infty}$, dimensionless

T   temperature, $^\circ F$ abs

v   velocity, ft/sec

φ angle with the longitudinal axis of the model, radians

γ ratio of specific heats (1.40 for air), dimensionless

μ viscosity, lb-sec/sq ft

ρ mass density, slugs/cu ft

Subscripts

n   conditions at the nose of the model

o   stagnation conditions

r   recovery conditions

D   referred to a characteristic diameter

∞ free-stream conditions

DESCRIPTION OF EQUIPMENT

Wind Tunnels

Three wind tunnels were used in the present investigation. The first was the Ames 6-inch heat transfer tunnel, a return-type, continuous operation tunnel. It is described in detail in reference 3. The second was the Ames 10- by 14-inch supersonic tunnel which is of the closed-jet nonreturn type. In addition to these, a 2- by 5-foot subsonic duct was used. This duct is of the nonreturn type and is powered by two variable-speed motors driving shrouded propellers mounted side by side.

Models

Photographs of the two heat-transfer models and the pressure distribution model employed in this investigation are shown in figure 1. The first heat-transfer model consisted of a 1-inch-diameter copper hemisphere mounted on a 5-1/2-inch-long stainless steel cylinder of the same diameter. A threaded orifice at the stagnation point of the hemisphere provided the means for attachment of the spikes. These spikes were 0.10 inch in diameter and of lengths 1/2, 3/4, 1, 1-1/2, and 2 inches. One end of each spike was threaded for attachment to the models; the other was machined to form a cone of 10° semiapex angle. In order to avoid conduction of heat along the spikes, they were made of Micarta which has a low value of thermal conductivity. When the spikes were not used, a small headless screw was used to plug the orifice in the model.

Power to the heat-transfer model was supplied by a 20-watt electric heater made by winding Advance wire about a small threaded Transite cylinder which was then fitted inside the hemisphere. Temperatures were measured by four iron-constantan thermocouples inserted in the nose within 1/16 inch of the surface at 90° intervals on a circle of 11/16-inch diameter concentric with the axis. A fifth thermocouple was placed within 1/8 inch of the stagnation point - as close as was possible without breaking through to the central orifice.

The hemispherical nose was attached to the cylindrical afterbody by means of a 2-1/4-inch-long, hollow, internal support shaft of stainless steel, 3/8 inch in diameter, which was passed through a 1/2-inch-long, 7/8-inch-diameter Micarta bushing threaded directly in the afterbody. In order to determine the axial heat conduction, three thermocouples were provided at equally spaced intervals along the axis of the support shaft. At the outer rim of the hemisphere, heat conduction to the stainless-steel afterbody was minimized by reducing the area of contact between these parts to less than 0.009 square inch. This was accomplished by chamfering the internal edge of the afterbody to a thickness less than 0.003 inch.

For a second series of tests the hemisphere consisted of two sectors which divided the surface area into halves. The copper frontal sector was heated as before while the stainless-steel rear segment was unheated. Heat flow to the latter segment was minimized by reducing the area of contact between the two sectors to less than 0.223 square inch. This was done by cutting wide annular grooves into the interior surfaces of the stainless-steel sector. Furthermore, the temperature difference between the two sectors could be measured since four thermocouples were placed at 90° circumferential intervals in each segment. From this model the average heat-transfer rate from the forward half-area of the hemisphere was found.

Pressure-distribution measurements were obtained with a separate stainless-steel nose. Sixteen pressure orifices (number 80 drill, 0.0135-inch diameter) were placed at 5° intervals with the longitudinal axis of the body from 15° to 85°. These holes were also displaced circumferentially from each other in a systematic fashion so that no two holes were on the same streamline (fig. 1(b)). In addition, each model was equipped with two pressure orifices placed diametrically opposite each other at an angle of 45° with the longitudinal axis in order to facilitate orientation to zero angle of attack. Stainless-steel tubes were soldered in the holes at the rear of the hemisphere and passed through the bushing into the cylindrical afterbody. There they were soldered to flexible copper tubes which connected to manometers outside the wind tunnel.

TEST PROCEDURE

The actual testing was divided into three phases: average heat-transfer and recovery-temperature tests for the entire hemisphere; the same tests for the frontal half-area of the hemisphere; and pressure-distribution tests.

Average heat-transfer rate and recovery temperature for the entire hemisphere were obtained by measuring the voltage and current to the heater, the body temperatures, and the stagnation temperature of the wind tunnel. All temperatures were obtained with iron-constantan thermocouples using the temperature of melting ice as a reference. They were read on an indicating potentiometer. Measurement of support-shaft temperatures enabled the determination of the amount of heat leakage along that member. During the initial tests, an air space of approximately 0.002 inch was maintained between the nose and the cylindrical afterbody preventing heat leakage in that direction. Later tests with the nose firmly in contact with the cylinder's chamfered edge revealed an increase in total heat leakage of less than 1 percent. All subsequent investigation was therefore conducted with the nose and afterbody in firm contact.

For each physical configuration (different length of spike) the power input to the heater was varied in six approximately equal steps from 0 to a maximum of almost 20 watts. A typical corresponding range of nose temperatures (depending on the Reynolds number) would be from 50° F to 160° F.

The phase of the investigation concerned with obtaining average heat transfer and recovery temperature over the frontal half-area of the hemisphere was conducted in the same manner as the first phase. Because the heat path for conduction between the hemisphere sectors was very small compared to the heat path for forced convection to the air stream, heat leakage between these sectors was neglected.

Pressure distributions were measured only at Mach numbers of 1.75 and 2.67. When no spike was attached, the pressure at the stagnation point ($\varphi = 0$) could be measured with the orifice then available at that point. However, when spikes were in place, the first station available for measurement was at $\varphi = \pi/12$ radians (15°).

The subsonic tests were conducted in the 2- by 5-foot duct, the supersonic tests at Mach numbers of 1.75 and 2.67 in the Ames 6-inch heat-transfer tunnel, and those at a Mach number of 5.04 in the Ames 10- by 14-inch supersonic tunnel.

DATA REDUCTION

Average heat-transfer coefficients and average recovery temperatures were found from the equation

$$Q = hA(T_r - T_n) \tag{1}$$

by the method of least squares using the six different sets of measured values of Q and T_n found for the six values of power input. An equivalent graphical method is to plot Q/A as a function of T_n; the heat-transfer coefficient then will be given by the slope and the recovery temperature will be found at the intercept where $Q/A = 0$. Over the range of temperatures used in this investigation (50° F to 190° F), it was found that the heat-transfer coefficient, h, was independent of the nose temperature. Therefore, in the above-mentioned graphical method, the data points formed a straight line.

In obtaining the heat transfer over the front half-area of the hemisphere, the same equations and the same procedure were used as for the entire hemisphere. Both of these sets of results were then employed to calculate the heat transfer for the rear half of the hemisphere by use of the equation

$$Nu_2 = 2Nu_t - Nu_1 \tag{2}$$

The subscripts 1, 2, and t refer to the front sector, rear sector, and total hemisphere, respectively. This equation was obtained from a simple heat balance assuming that both segments have the same average recovery temperature. The average recovery temperature can be defined as the temperature assumed by the nose when the net rate of heat flow to or from the nose is zero.

The pressure drag of the unspiked hemisphere was calculated by integrating the pressure distribution about the nose using the expression

$$D = \frac{\pi}{2} \, d^2 \int_0^{\pi/2} P \sin \varphi \cos \varphi \, d\varphi \qquad (3)$$

The drag coefficient was based on the projected frontal area of the model and thus was calculated from

$$C_D = \frac{4}{\gamma P_\infty M_\infty^2} \int_0^{\pi/2} P \sin \varphi \cos \varphi \, d\varphi \qquad (4)$$

When spikes were attached to the nose of the model, the lower limit of integration was changed to exclude the frontal area of the spike. The theoretical pressure drag on a 10° cone as obtained from reference 5 was added to obtain the total pressure drag of the hemisphere-spike combination. In all cases the skin friction along the spike was neglected.

<center>DISCUSSION OF RESULTS</center>

According to Fage (ref. 6), the point of transition from laminar to turbulent flow in the boundary layer of a sphere always occurs on the rear hemisphere at Reynolds numbers from 1.57×10^5 to 4.24×10^5. Since the Reynolds numbers of Fage's experiments correspond closely to those of the present tests (based on conditions behind the normal bow shock wave), the boundary layer on the unspiked hemisphere can be assumed laminar.

The experimentally determined values of average heat transfer for the unspiked hemisphere are shown in figure 2. It is to be noted that when the air-stream properties are evaluated behind the normal shock wave, there is excellent correlation between the supersonic and subsonic results of this experiment. Thus it is possible to predict supersonic heat transfer for this configuration from the subsonic data.

Since the average heat transfer from a hemisphere cannot be correlated directly with that from a sphere (due to the phenomenon of separation), only a limited amount of data is available for comparison with the present results in figure 2. There were three subsonic tests which involved an identical experimental technique; namely, passing steam through a hollow sphere, balancing the temperature of a small independently heated plug to that of the remainder of the sphere, and measuring the power input to the plug, thus determining the local heat transfer to the air stream. The values thus found may then be integrated over the surface of the front half of the sphere to obtain average heat-transfer coefficients.

The first of these tests was conducted by Lautman and Droege (ref. 7) who, in 1950, obtained Nusselt numbers for the front half of a sphere which are approximately 50 percent above those obtained in the present experiment. Their work, however, was superseded by that of Xenakis, Amerman, and Michelson (ref. 8) who tested the same model (along with two other spheres of different dimensions) but improved the instrumentation. The latter used values of the thermal conductivity of air based on an average of the wall and air temperatures. Therefore, it was necessary to adjust their Nusselt numbers to free-stream values in order to enable comparison with the present work. Unfortunately, neither the air-stream temperatures nor the ambient (stagnation) temperatures were given in reference 8, so it was also necessary to estimate the stagnation temperature. On the basis of the available information, a value of 60° F was estimated. The resulting Nusselt numbers are approximately 20 percent higher than those found in the present work. The discrepancy may possibly be due to two sources of error which were not evaluated sufficiently in reference 8. The first was the use of "cross-wind" supports in mounting the models in the wind tunnel; the second was the use of guy wires which were attached to the supports just below the models. The effects of these methods of support on the air flow about a sphere are not negligible (ref. 9) and may easily contribute to an increase in heat transfer from the sphere.

The third test was conducted by Cary (ref. 10) who obtained local values about a sphere which, when integrated over the front half are approximately 50 percent below those obtained in this investigation. The reasons for the great discrepancy between Cary's results and those of references 7 and 8 are not known and cannot be determined from the information in reference 10. It is noteworthy, however, that a thin-shelled iron sphere was used instead of a copper one as in the other tests. The presence of a condensation film within this sphere would quite likely produce nonuniform surface temperatures which would greatly affect the heat-transfer data.

Korobkin (ref. 11) presents experimental results obtained for a hemisphere-cylinder in a supersonic blow-down wind tunnel which are below those of this experiment. However, his data are admittedly in error due to axial conduction of heat in the model. When his experimental data are corrected as described in reference 11, they are in essential agreement with the present data. Korobkin also used unpublished results of Sibulkin to obtain a theoretical solution for local heat transfer about a hemisphere. When this is adjusted to the exact solution at the stagnation point (ref. 12), it results in a curve of $Nu_D Re_D^{-1/2}$ about a hemisphere which, when integrated, corresponds very closely with the present results.

The reasons for the discrepancy between the results of previous investigations is difficult to establish because of the lack of information concerning probable sources of experimental errors. It is thought, however, that the present data, which are in essential agreement with

the corrected results of Korobkin, can be used with confidence in view of the fact that they were obtained in three different wind tunnels under widely different conditions of Mach number and wind-tunnel configuration.

Figures 3(a) and 3(b) show average temperature-recovery factors as a function of free-stream Reynolds number. It can be seen that the temperature-recovery factor decreases with the addition of spikes. Over the range of spike lengths tested, it was found that as the spike length was increased, the temperature-recovery factor decreased. At a Mach number of 1.75, the 2-inch spike reduced the recovery factor by 3 to 5 percent; at a Mach number of 2.67, the reduction was from 5 to 10 percent. In terms of flight conditions this means that at an altitude of 100,000 feet and a Mach number of 2.67, a missile approximately 1 foot in diameter equipped with a spike would have an equilibrium nose temperature of 365° F, while a missile without a spike would be approximately 40° F warmer. It is interesting to note that an increase in Mach number increases the recovery factor of the unspiked hemisphere but appears to have relatively little effect on the recovery factor of a hemisphere equipped with spikes.

The effect on Nusselt number of installing spikes in front of a hemisphere is shown in figures 4(a) to 4(c). For given values of Mach number and Reynolds number, regardless of spike length, the rate of heat transfer is almost double that obtained on unspiked hemispheres. This was also found to be true when a blunt disk or cone was substituted for the point of the spike (fig. 4(b)). Figure 4(c) shows Nusselt number as a function of Mach number for spiked and unspiked hemispheres at a Reynolds number of 3.35×10^5. It may be seen from this figure that the Nusselt number of the spiked body is approximately double that of the unspiked body, regardless of Mach number.

A more local determination of the effect of spikes on heat transfer was obtained with the model which separated the hemisphere into two surfaces of equal area. Figure 5 presents Nusselt number as a function of Reynolds number for the two sectors of the hemisphere with and without spikes at a Mach number of 2.67. It is noteworthy that the addition of spikes increases the heat transfer from the leading half of the hemisphere almost exclusively. There is relatively little effect on the heat transfer from the trailing half of the hemisphere.

Although the physical explanation for the increase in heat transfer when spikes are attached to the nose is not known, some indication of the mechanism involved may be obtained from a study of selected shadowgraphs (figs. 6 to 11) in conjunction with the pressure distribution shown in figure 12. From the shadowgraphs it can be seen that the volume bounded by the nose, the spike, and the main air stream is one of extreme turbulence. A qualitative indication of the intensity can be obtained by comparison with the turbulent boundary layer of the wind-tunnel wall which is visible at the bottom of each picture. In figure 12, a typical

plot of the pressure distribution about the spiked configuration is superimposed on the pressure distribution about an unspiked hemisphere. The reversals of slope, which are representative of all the pressure distributions of the spiked hemispheres, indicate reversal of the direction of flow along the surface. Furthermore, the steep pressure gradients signify a tendency toward velocities of large magnitudes. Thus the term "dead-air region" as applied to this space by previous investigators (refs. 1 and 2) is apparently a misnomer. However, this turbulence in the separated region is not sufficient evidence to attribute the increased heat transfer due to spikes to turbulence in the boundary layer. Flat-plate data, which are qualitatively applicable to the present case, show that the rate of heat transfer through a fully developed turbulent boundary layer is from four to five times greater than that through a laminar boundary layer (ref. 13). In addition, the increase of Nusselt number with Reynolds number is 60 percent more rapid for turbulent than for laminar boundary layers. The addition of spikes does not produce changes of these magnitudes. It is conjectured that the increased heat transfer due to spikes may be caused by repeated impingement of the turbulent separated region into the outer edge of the boundary layer on the body nose. This conjecture seems consistent with the observed fact that the increase in heat transfer is independent of the spike length. However, further investigation is necessary before a definite opinion can be ventured.

Figures 13(a) and 13(b) show pressure drag coefficient as a function of the ratio of spike length to body diameter. As the length of the spike is increased, the drag coefficient decreases, reaches a minimum, and then appears to rise again.

It can be seen from figures 6 through 9 that the region of separated flow appears to have the general shape of a cone. The apex angle of the cone formed by the separated region varied as the spike length was increased. Within the range of probe lengths tested, the drag varied in the same manner as the apex angle. By comparison of figures 6 to 8 with figure 13(b) it can be seen that the drag coefficient decreased as this apex angle became narrower and, in turn, increased as the angle again widened.

The flow separation and the attendant drag reduction are obviously consequences of shock-wave interaction with the boundary layer on the spike. The process has been described in part by Mair as follows: At supersonic speeds the rise of pressure across the bow shock wave in front of a blunt body causes separation of the boundary layer on the spike. The separated boundary layer spreads downstream forming an approximately conical region. The resulting distortion of the streamlines outside the region produces a positive pressure gradient on the spike, and the vertex of the conical separated boundary layer moves upstream until a point of equilibrium is reached. Any further forward movement results in a decrease in cone angle which decreases the angle of the shock wave to the point where the pressure rise across the shock wave is insufficient to maintain separation.

For the shorter spikes, separation occurs at the tip (fig. 6). As the spike length is increased, the separation point moves back to the shoulder and remains there through a range of lengths. Therefore, as the spike length is increased, the vertex angle of the separated region decreases and, correspondingly, the drag decreases. (Figure 7 shows a typical example of separation at the shoulder of the spike.) This decrease continues until the separation point leaves the shoulder to move downstream along the spike (fig. 8(a)). Then the vertex angle of the separated region increases and again, correspondingly, the drag increases. From the data and photographs obtained in this experiment, it can be concluded that the minimum drag is obtained with the longest conical-tipped spike for which separation will occur at the shoulder.

The curves of figure 13 may be misleading since the apparent upward trend of the drag is not expected to continue. It is believed that two flow-separation regions, laminar and turbulent, are represented and that the curve of drag coefficient as a function of spike length consists of two branches connected by a transition zone. The present data extend just through this transition zone and it is believed that the use of spikes with length to body-diameter ratio above 2 will not greatly increase the pressure drag of the configuration beyond the values shown. This belief is based on Mair's observations which indicate that when the boundary layer on the spike is turbulent, the position of the separation point and, thus, the flow about the hemisphere are relatively independent of spike length.

The qualitative differences between the separation of laminar boundary layers and turbulent boundary layers can be seen in figures 8 and 9. In the latter case, the boundary layer was tripped by a ring of carborundum dust at the shoulder of the spike and can be assumed turbulent. In figure 8(a), on the other hand, the short length of boundary-layer run leads one to expect that at least this photograph illustrates separation of a laminar boundary layer. Thus figures 8(b) and 8(c) also probably illustrate laminar separation. Since these three photographs were taken within a few seconds of each other, it can be seen that the separation point was apparently oscillating along the length of the spike. Whether this oscillation is inherent or is caused by bursts of turbulence in the free stream is not known. Oscillation has also been observed, however, by Mair (ref. 1) who attributes it to wind-tunnel disturbances. The separation point of the turbulent boundary layer of figure 9 exhibited no oscillation, again verifying observations by Mair.

Other differences between laminar and turbulent separation are manifest in the shock-wave patterns of figures 8 and 9. In figures 8(a) to 8(c), a complicated shock system has been established. The pressure rise across the main bow shock wave has been transmitted upstream through the boundary layer, causing separation to occur on the spike. At the point of separation a weak conical shock wave is formed which has a pressure rise just sufficient to maintain separation. It is shown in reference 14 that the value of the critical pressure coefficient across

a shock wave which will separate a turbulent boundary layer on a flat
plate is approximately five to ten times as great as that required when
the boundary layer is laminar. Thus it is to be expected that separation
of a turbulent boundary layer will be accompanied by a much stronger
conical shock wave than will separation of a laminar boundary layer.
This hypothesis is substantiated by comparison of figures 8 and 9.

Returning to figures 8(a), 8(b), and 8(c), it should be noted that
there is a sharply defined light line at the edge of the separated region
in each photograph extending a few spike diameters downstream of the
separation point. This line indicates that the boundary layer probably
remained laminar for this distance after separation. Farther downstream
the line becomes indistinct as the boundary layer probably becomes tur-
bulent. This transition appears to be accompanied by the formation of a
secondary shock wave which is also oscillatory. In figure 8(a), the
secondary shock wave is approximately conical. In figures 8(b) and 8(c),
however, the shock waves are closer to the body and exhibit definite
curvature.

CONCLUSIONS

Measurements were made on the nose of a hemisphere-cylinder with
and without flow-separation spikes over a range of Mach numbers from
0.12 to 5.04 and Reynolds numbers from 1.55 to 9.85×10^5. These measure-
ments lead to the following conclusions:

1. For an unspiked hemisphere, the heat transfer at supersonic
speeds can be predicted from data obtained at subsonic speeds by evalu-
ating the air-stream properties behind the normal shock wave.

2. In supersonic flow the addition of conical-tipped spikes to a
hemispherical-nosed body with a laminar boundary layer approximately
doubles the average heat-transfer rate, regardless of spike length.

3. Almost the entire increase in the heat transfer due to the addi-
tion of spikes occurs over the forward half of the surface area of the
hemisphere.

4. On the addition of spikes at Mach numbers of 1.75 and 2.67, the
temperature-recovery factors decreased from 3 to 5 percent and from 5 to
10 percent, respectively, depending on the Reynolds number. The longer
the spike, the greater was the reduction obtained.

5. The addition of spikes reduced the pressure drag of the body approximately 45 percent for the best configuration. The minimum drag was obtained with the longest spike on which separation occurred at the shoulder.

Ames Aeronautical Laboratory,
    National Advisory Committee for Aeronautics,
   Moffett Field, Calif., July 13, 1954.

REFERENCES

1. Mair, W. A.: Experiments on Separation of Boundary Layers on Probes in Front of Blunt-Nosed Bodies in a Supersonic Airstream. The Philosophical Magazine, vol. 43, no. 342, July 1952, pp. 695-716.

2. Moeckel, Wolfgang E.: Flow Separation Ahead of Blunt Bodies at Supersonic Speeds. NACA TN 2418, 1951.

3. Stalder, Jackson R., Rubesin, Morris W., and Tendeland, Thorval: A Determination of the Laminar-, Transitional-, and Turbulent-Boundary-Layer Temperature-Recovery Factors on a Flat Plate in Supersonic Flow. NACA TN 2077, 1950.

4. Eggers, A. J., Jr., and Nothwang, George J.: The Ames 10- by 14-Inch Supersonic Wind Tunnel. NACA TN 3095, 1954.

5. Kuethe, Arnold Martin, and Schetzer, Julius David: Foundations of Aerodynamics. John Wiley and Sons, Inc., New York, 1950, pp. 171-172.

6. Fage, A.: Experiments on a Sphere at Critical Reynolds Numbers. Aeronautical Research Committee, R. & M. No. 1766, British A.R.C., 1937.

7. Lautman, Lester G., and Droege, William C.: Thermal Conductances About a Sphere Subjected to Forced Convection. Smith, Hinchman, & Grylls, Inc., Aero. Ice Res. Lab., ser. no. AIRL A6118, 50-15-3, Aug. 1950.

8. Xenakis, G., Amerman, A. E., and Michelson, R. W.: An Investigation of the Heat-Transfer Characteristics of Spheres in Forced Convection. Wright Air Development Center Rep. 53-117, Apr. 1953.

9. Goldstein, Sydney, ed.: Modern Developments in Fluid Dynamics. Second ed., vol II, The Clarendon Press, Oxford, 1938, pp. 493-494.

10. Cary, John R.: The Determination of Local Forced-Convection
       Coefficients for Spheres. Trans. ASME, vol. 75, no. 4, May 1953,
       pp. 483-487.

11. Korobkin, Irving: Local Flow Conditions, Recovery Factors and Heat-
       Transfer Coefficients on the Nose of a Hemisphere-Cylinder at a
       Mach Number of 2.8. U. S. Naval Ordnance Lab., NAVORD Rep. 2865,
       May 1953.

12. Sibulkin, M.: Heat Transfer Near the Forward Stagnation Point of a
       Body of Revolution. Jour. Aero. Sci., vol. 19, no. 8, Aug. 1952,
       pp. 570-571.

13. Slack, Ellis G.: Experimental Investigation of Heat Transfer
       Through Laminar and Turbulent Boundary Layers on a Cooled Flat
       Plate at a Mach Number of 2.4. NACA TN 2686, 1952.

14. Lange, Roy H.: Present Status of Information Relative to the
     · Prediction of Shock-Induced Boundary-Layer Separation.
       NACA TN 3065, 1954.
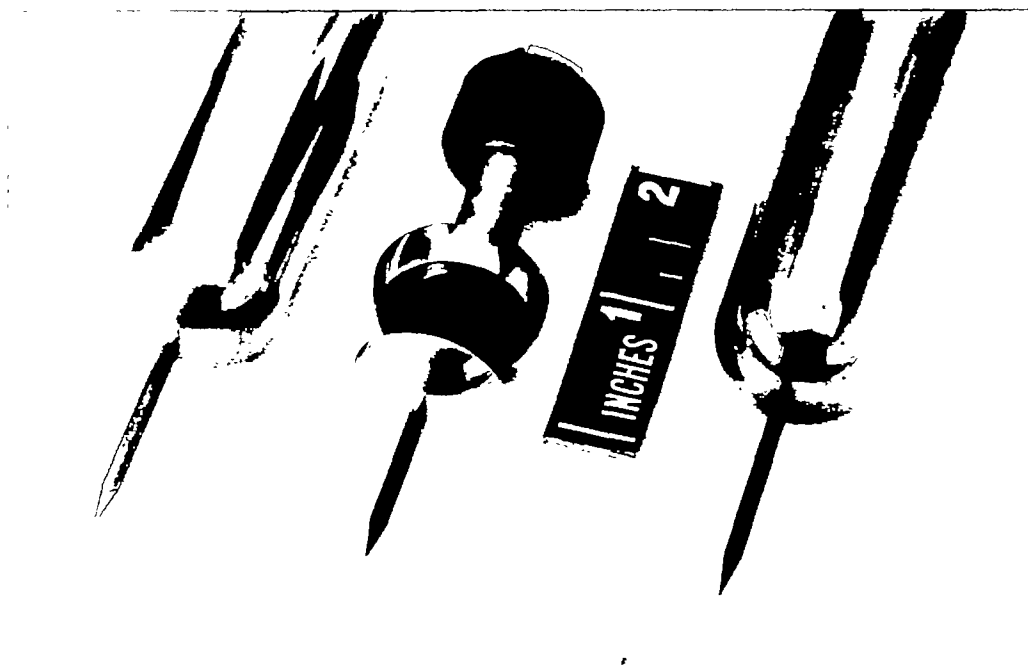
A-19019

(a) From left to right: heat-transfer model with copper nose, segmented nose, and the pressure-distribution model.
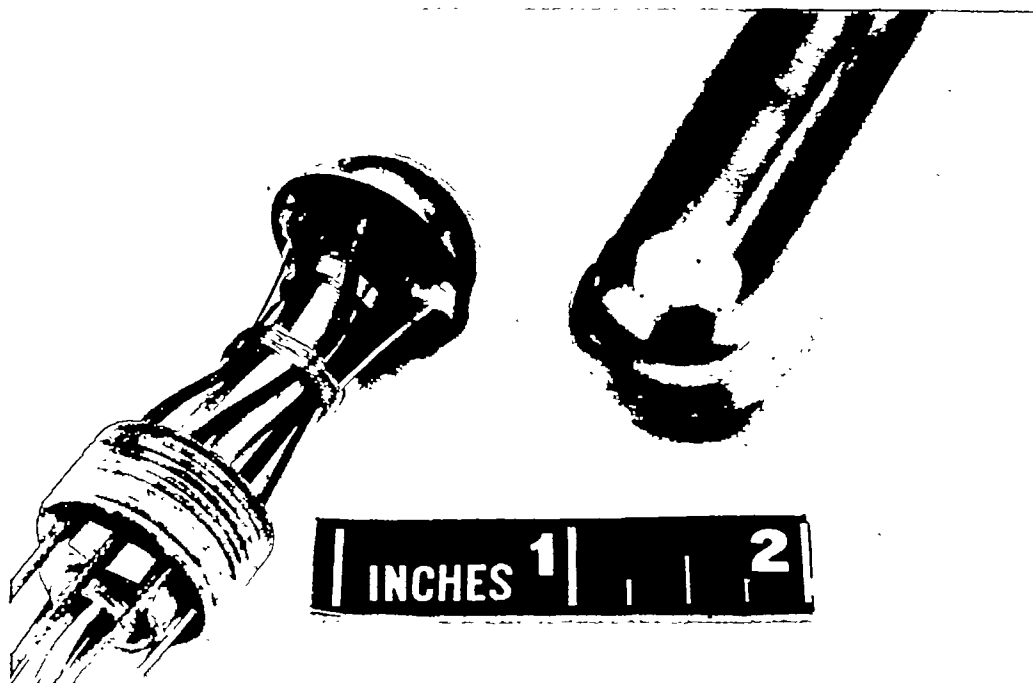
A-19020

(b) Thermocouple installation in heat transfer model and orifice distribution in pressure model.

Figure 1.- General view of models tested.
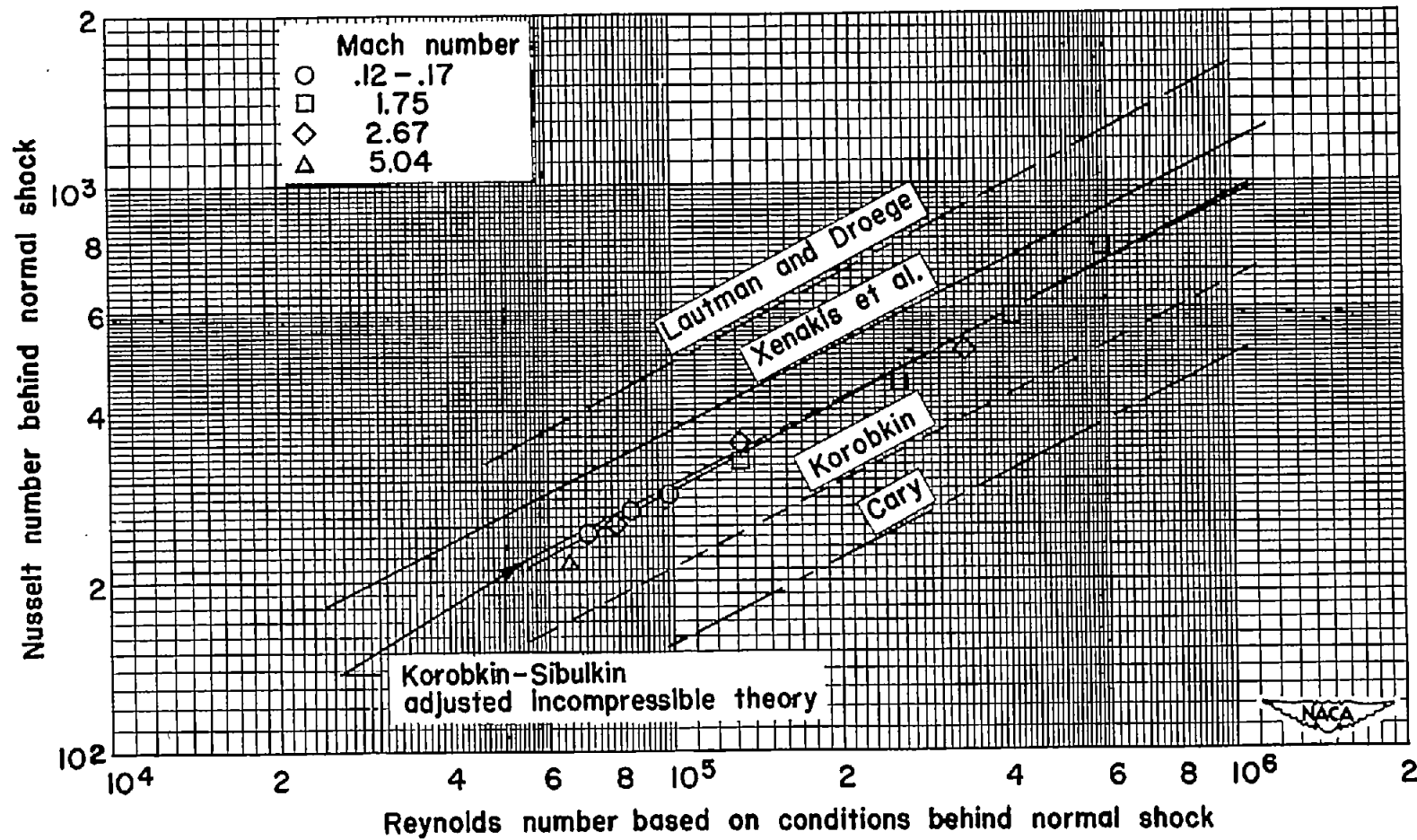
Figure 2.- Average heat transfer from hemispherical nose.
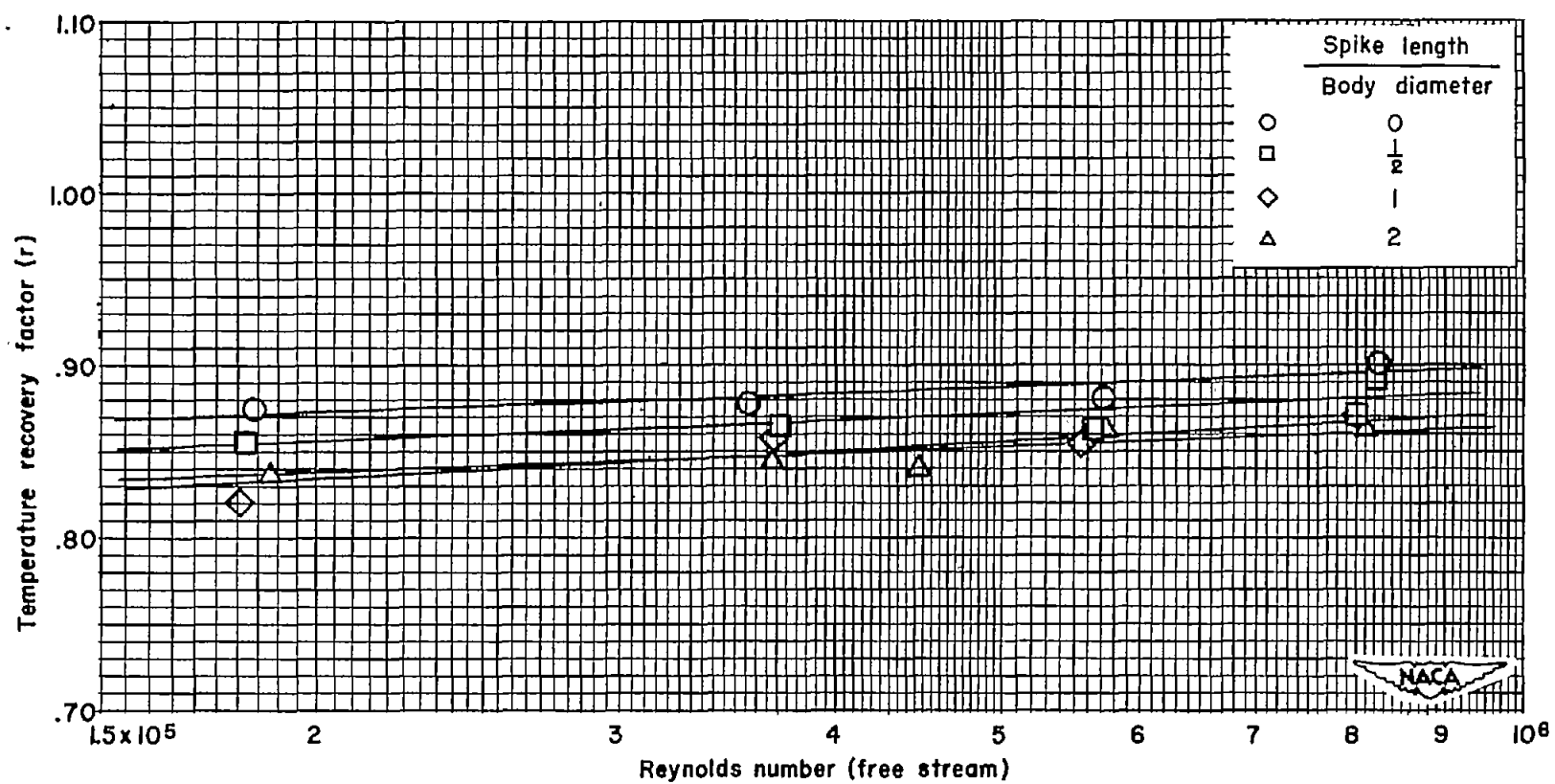
(a) M = 1.75

Figure 3.- Average temperature-recovery factor for hemispherical nose.
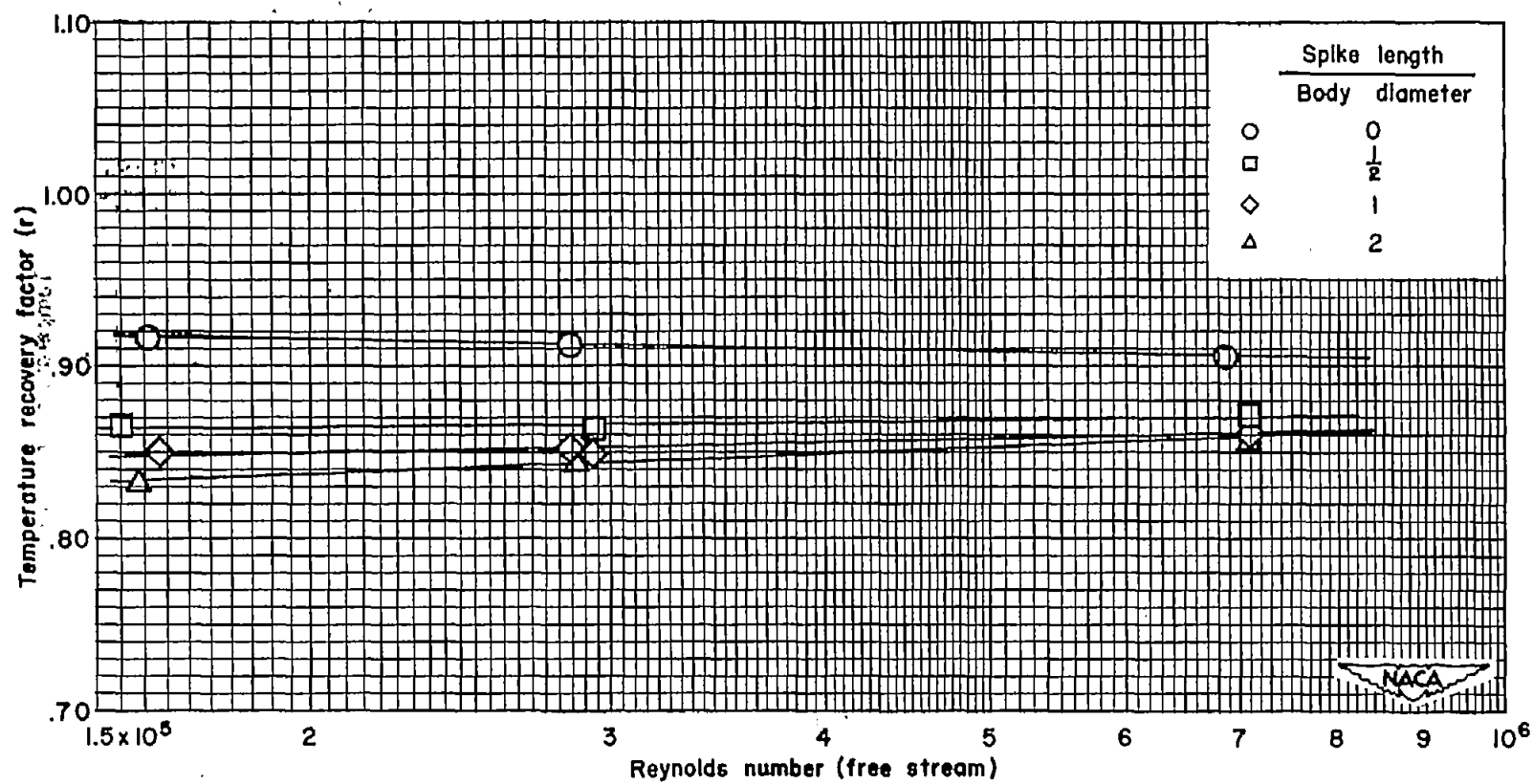
(b) M = 2.67

Figure 3.- Concluded.
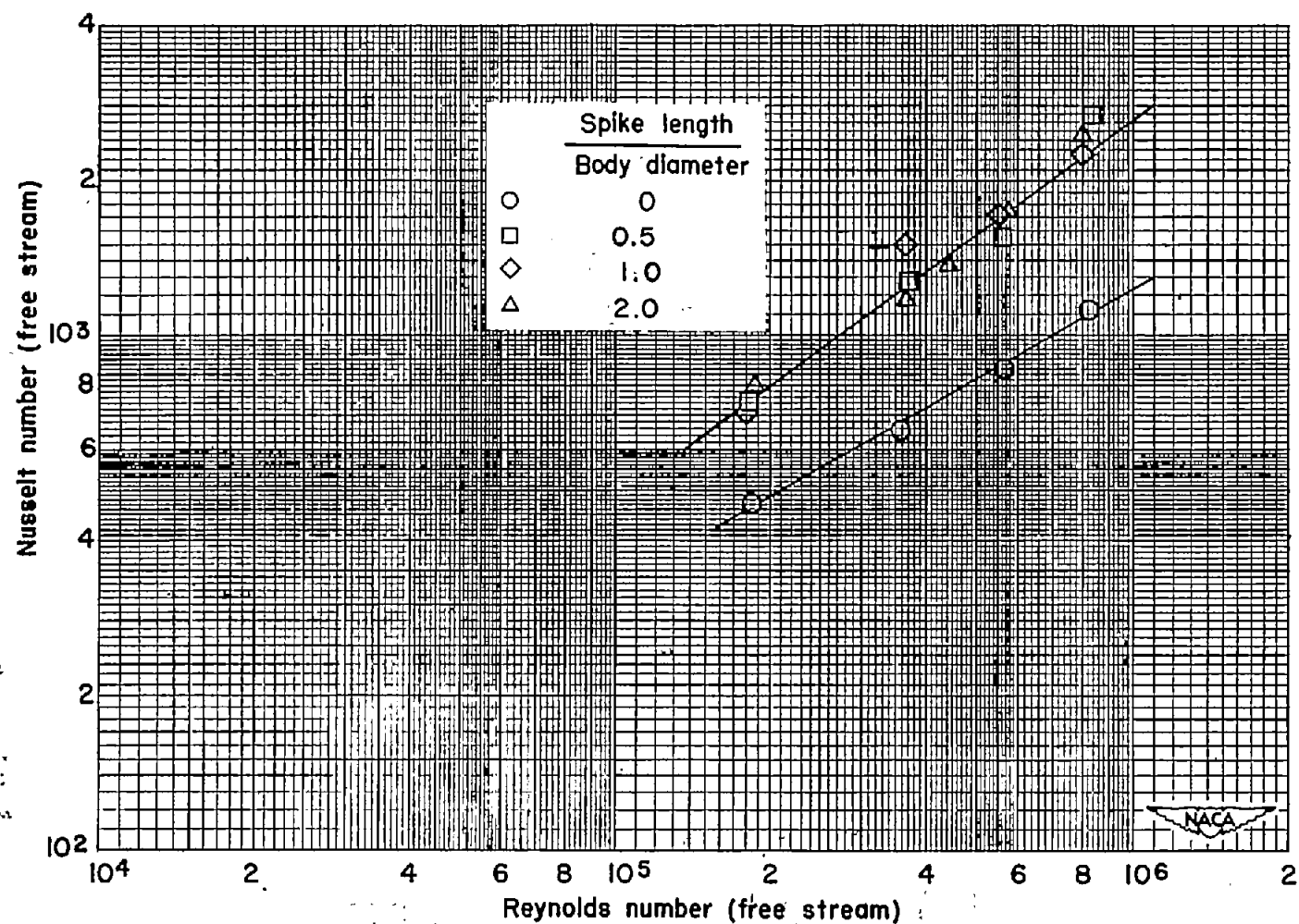
(a) Effect of spikes at M = 1.75.

Figure 4.- Average heat transfer from hemispherical nose with and without spikes.
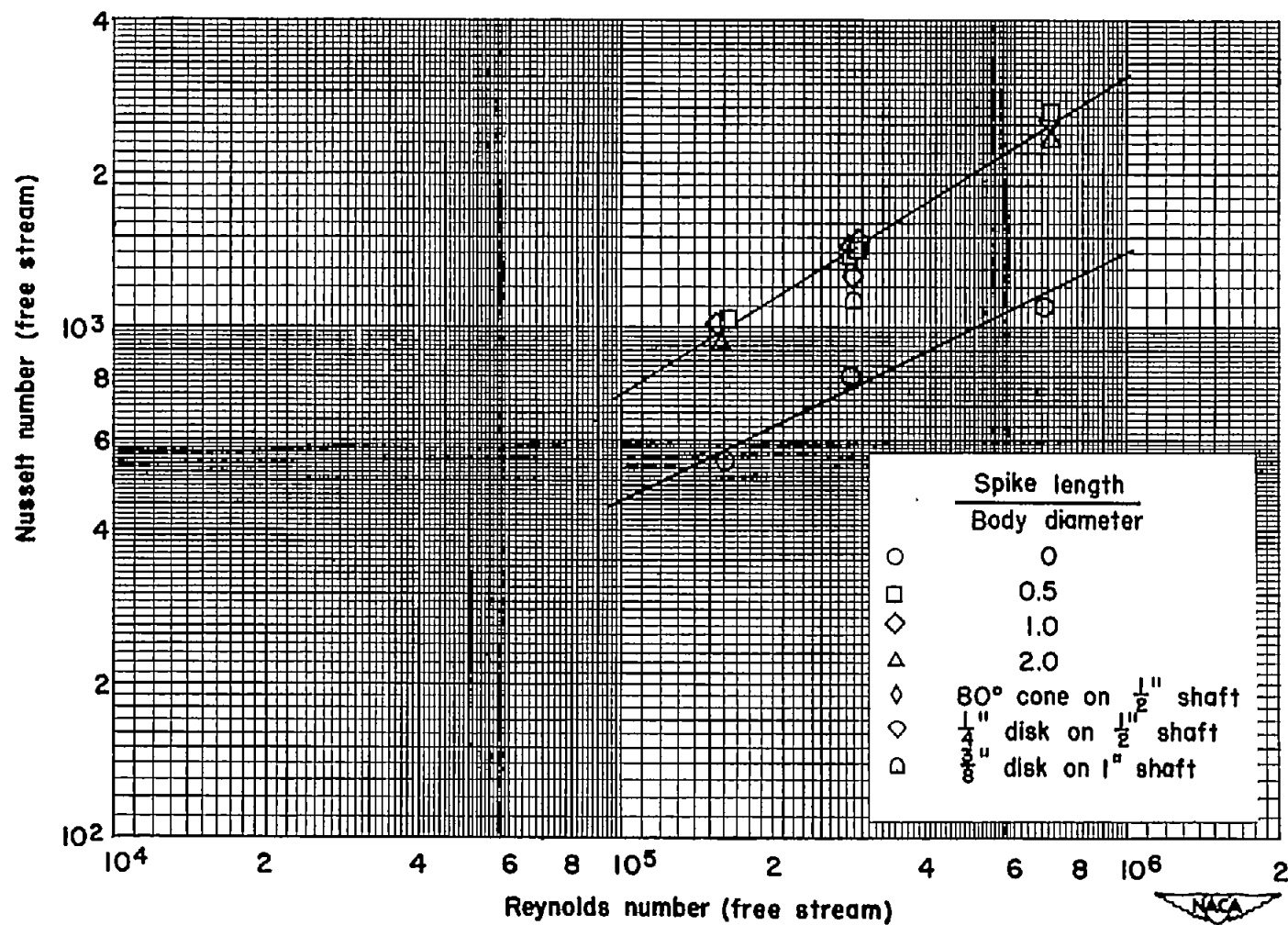
(b) Effect of spikes at M = 2.67.

Figure 4.- Continued.
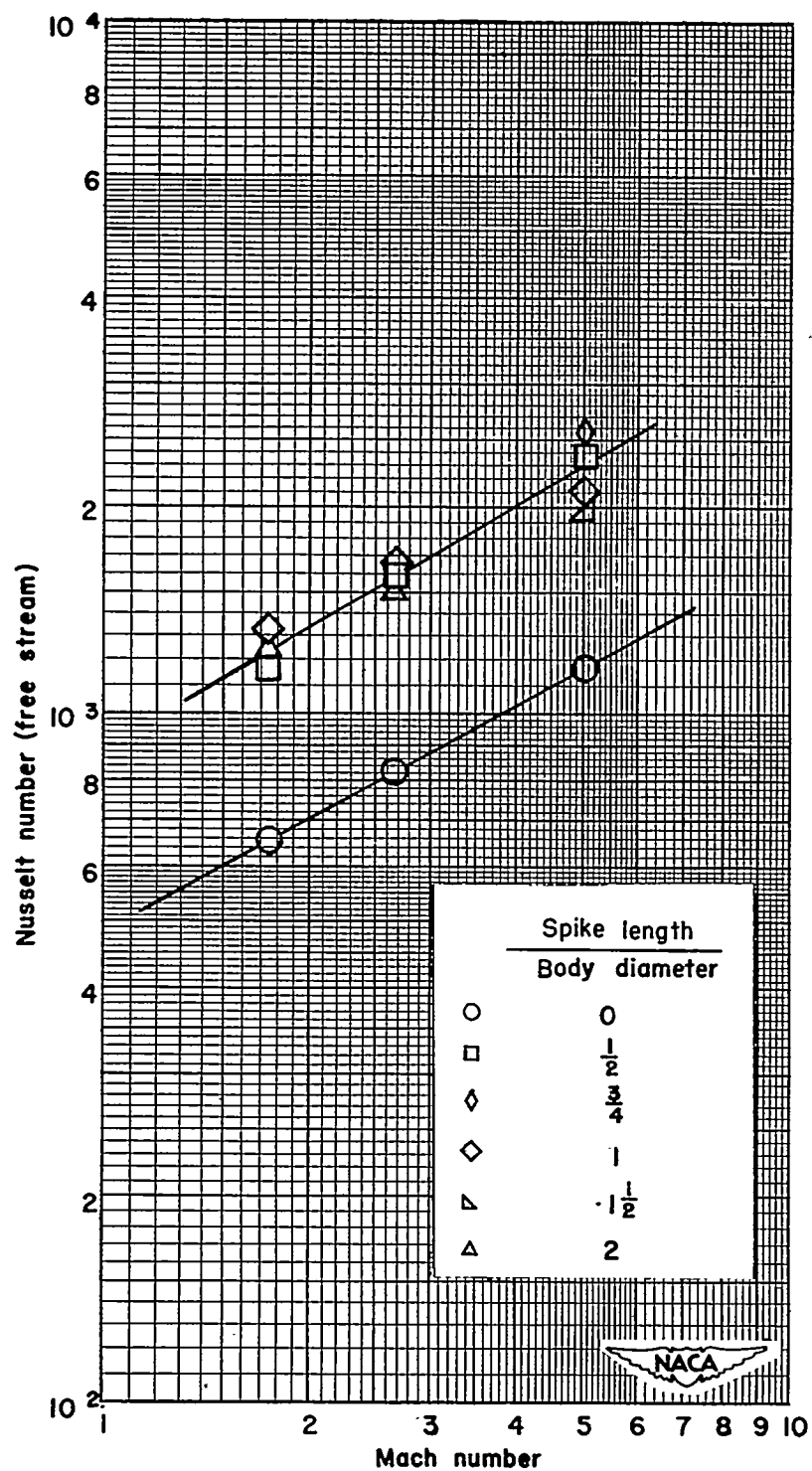
(c) Effect of Mach number at $Re_D = 3.35 \times 10^5$.

Figure 4.- Concluded.
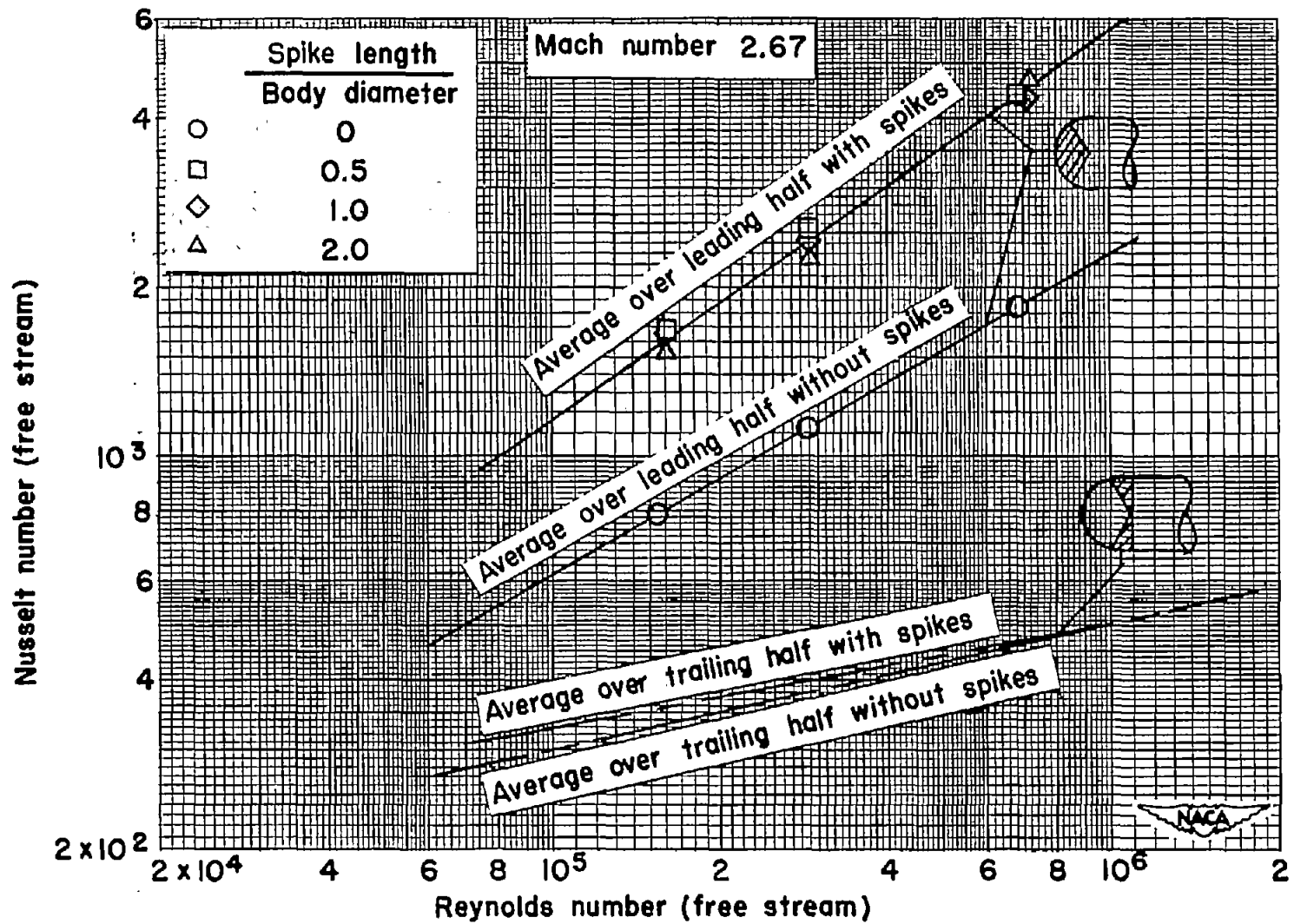
Figure 5.- Average heat transfer from half-area model.
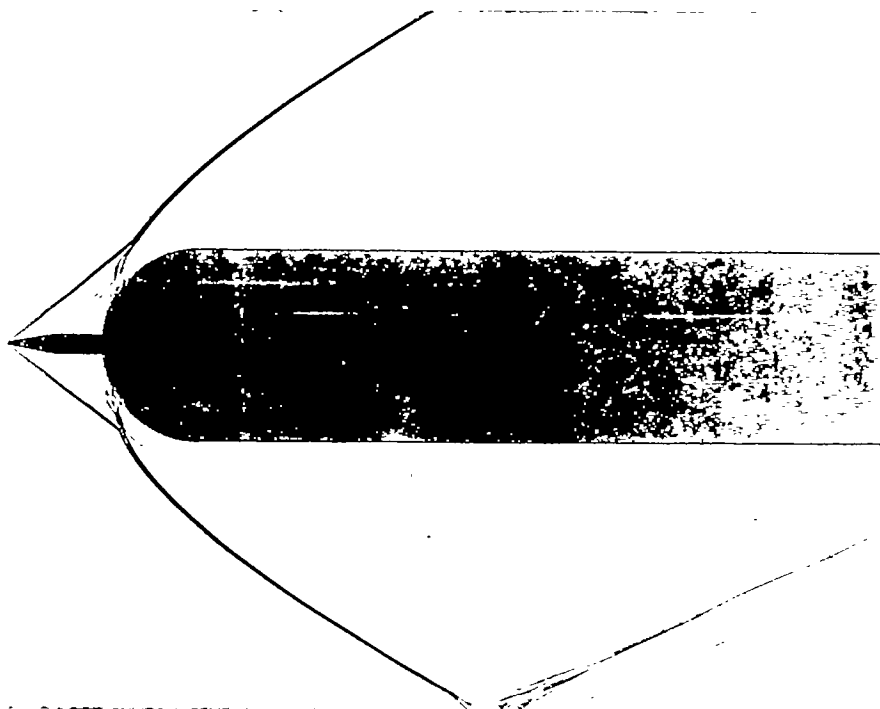
A-19089

Figure 6.- One-half inch spike; $M = 2.67$, $Re_D = 7.09 \times 10^5$.
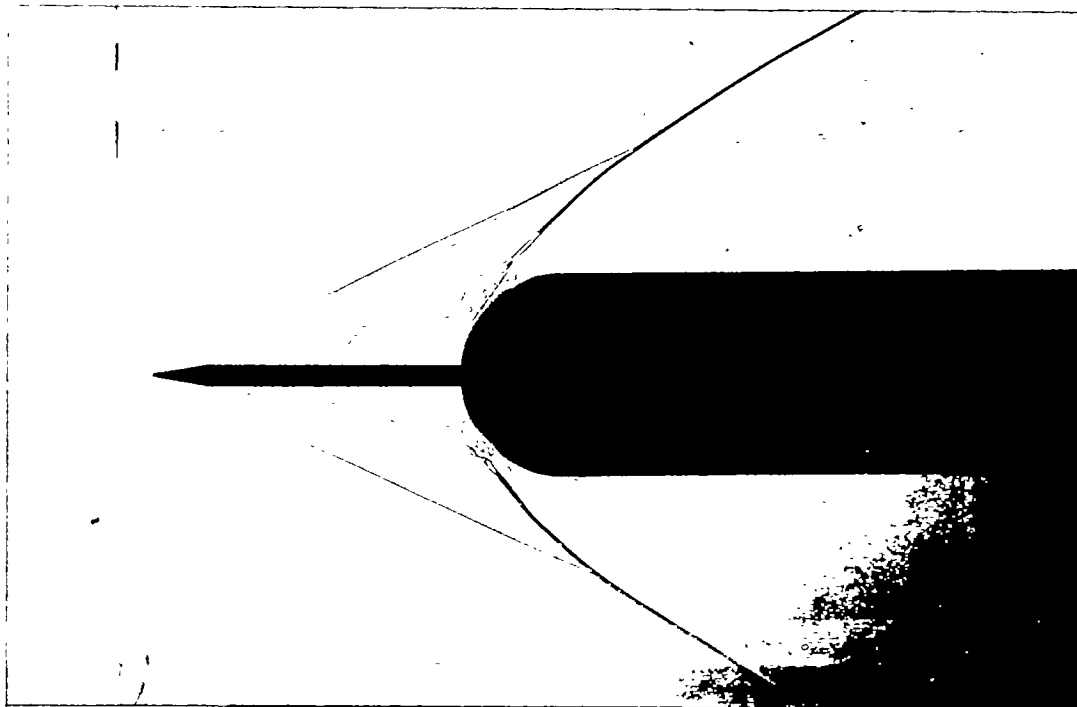
A-19243

Figure 7.- One and one-half inch spike; $M = 2.67$, $Re_D = 7.09 \times 10^5$.
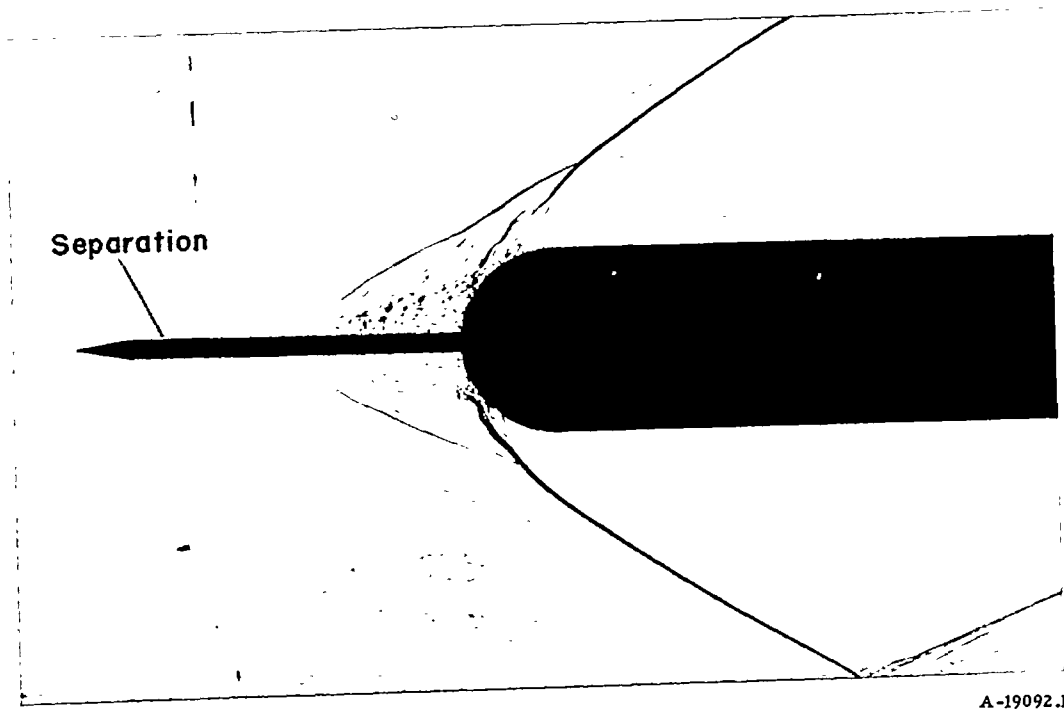
(a)   Separation point 0.45 inch from tip.
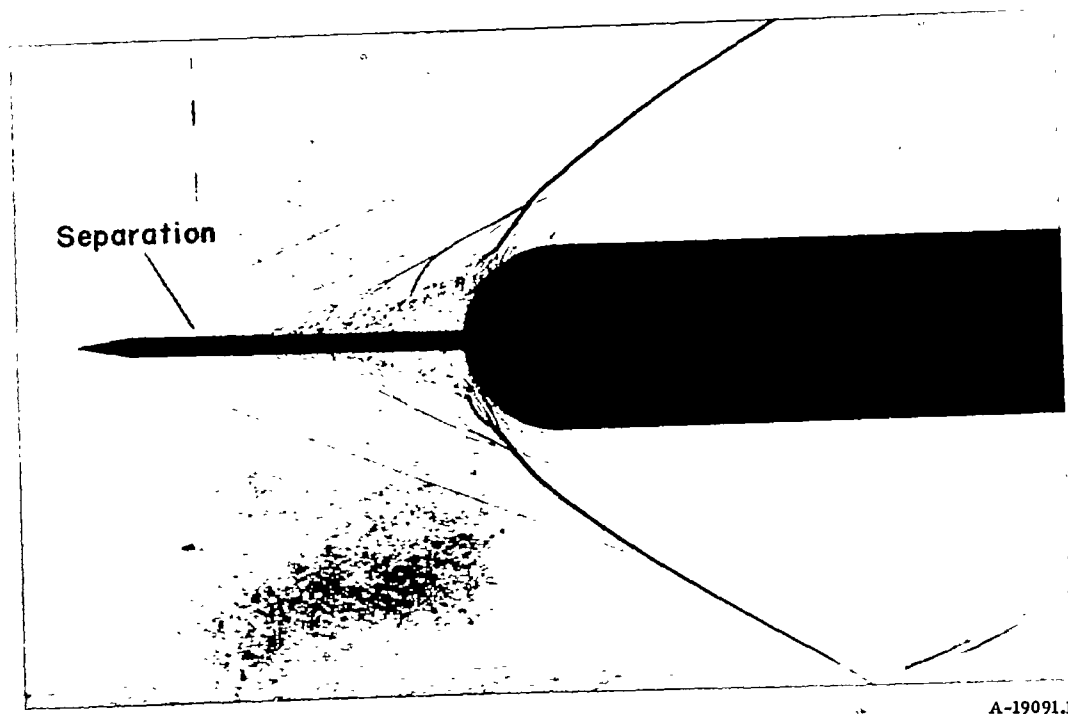
(b)   Separation point 0.60 inch from tip.

Figure 8.- Two-inch spike; $M = 2.67$, $Re_D = 7.09 \times 10^5$.
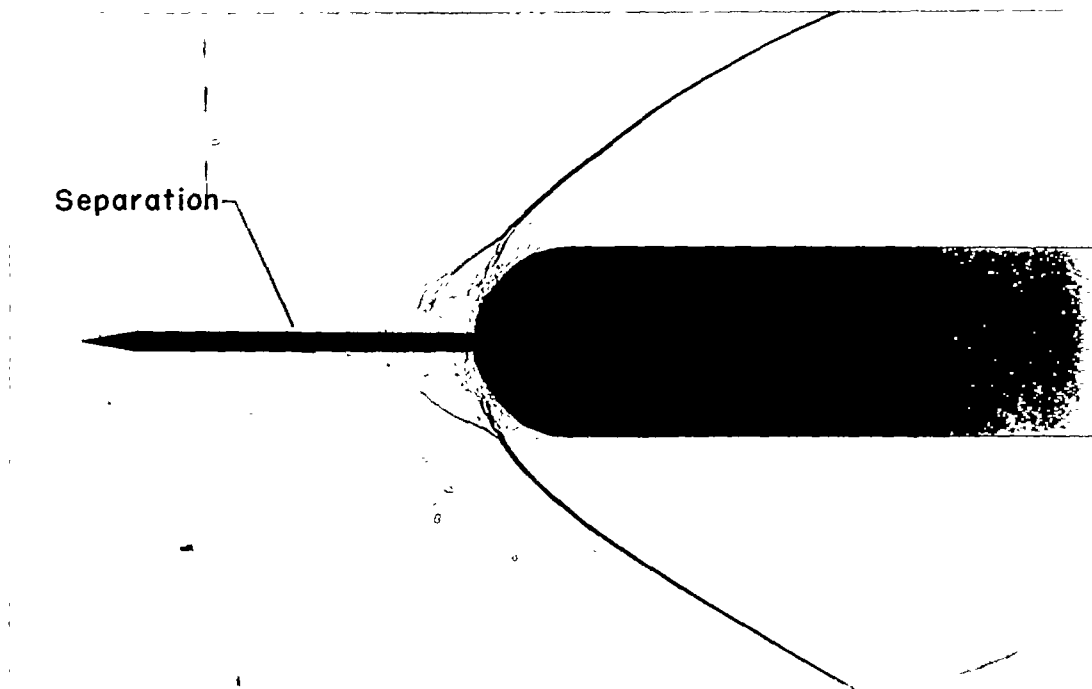
(c)   Separation point 1.06 inch from tip.

A-19093.1

Figure 8.- Concluded.
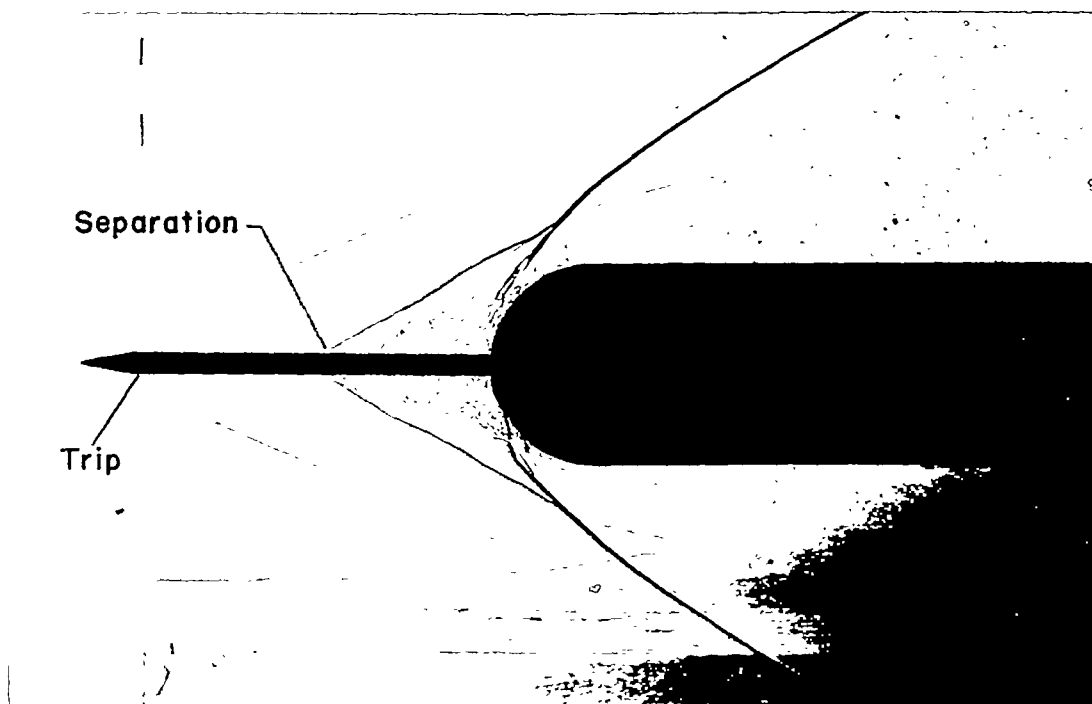
A-19244.1

Figure 9.- Two-inch spike with boundary-layer trip; M = 2.67,
$Re_D = 7.09 \times 10^5$.
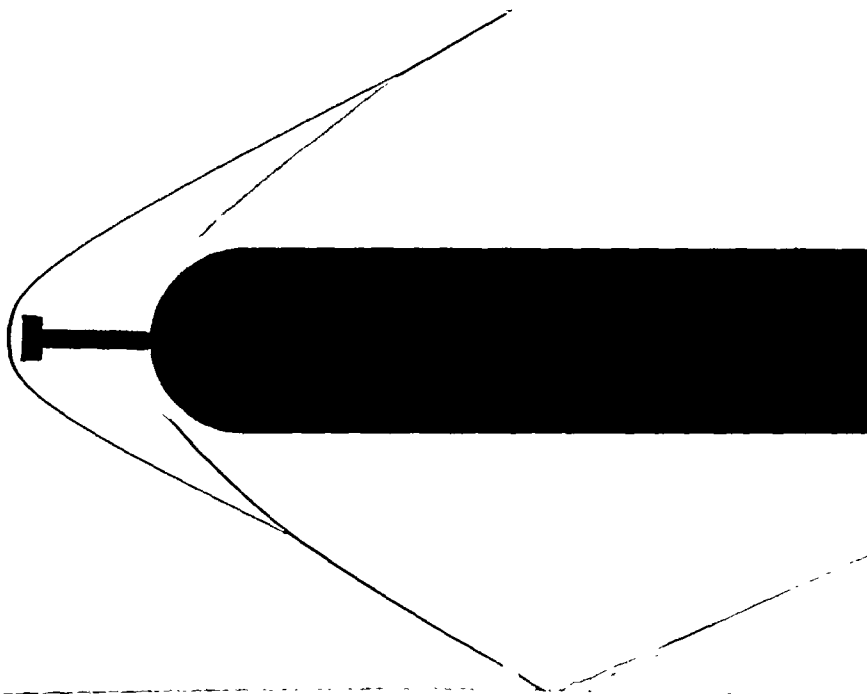
A-19095

Figure 10.- Blunt disk extending 3/4 inch in front of body; M = 2.67,
$Re_D = 2.90 \times 10^5$.
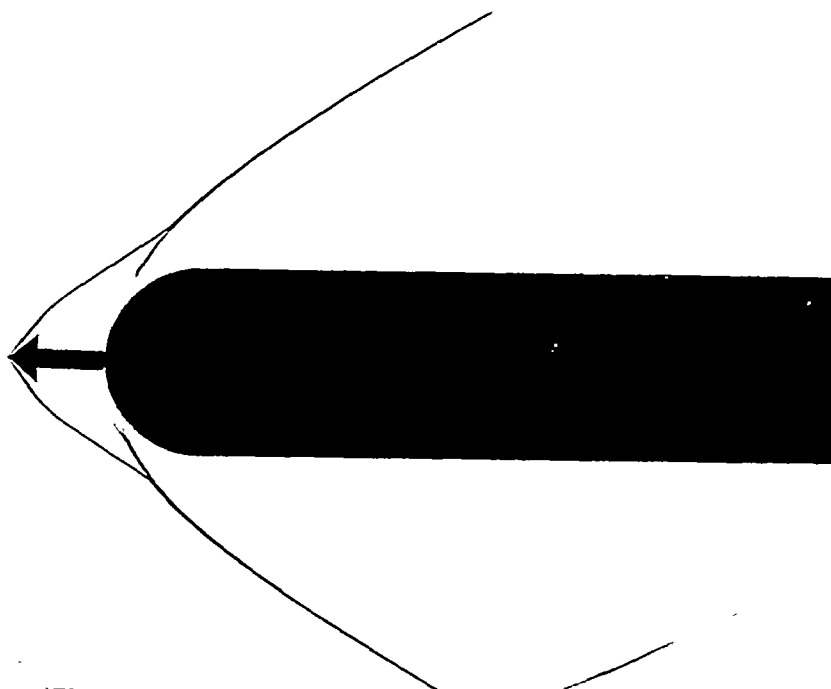
A-19096

Figure 11.- Blunt cone ($40°$ semiapex angle) extending 1/2 inch in front
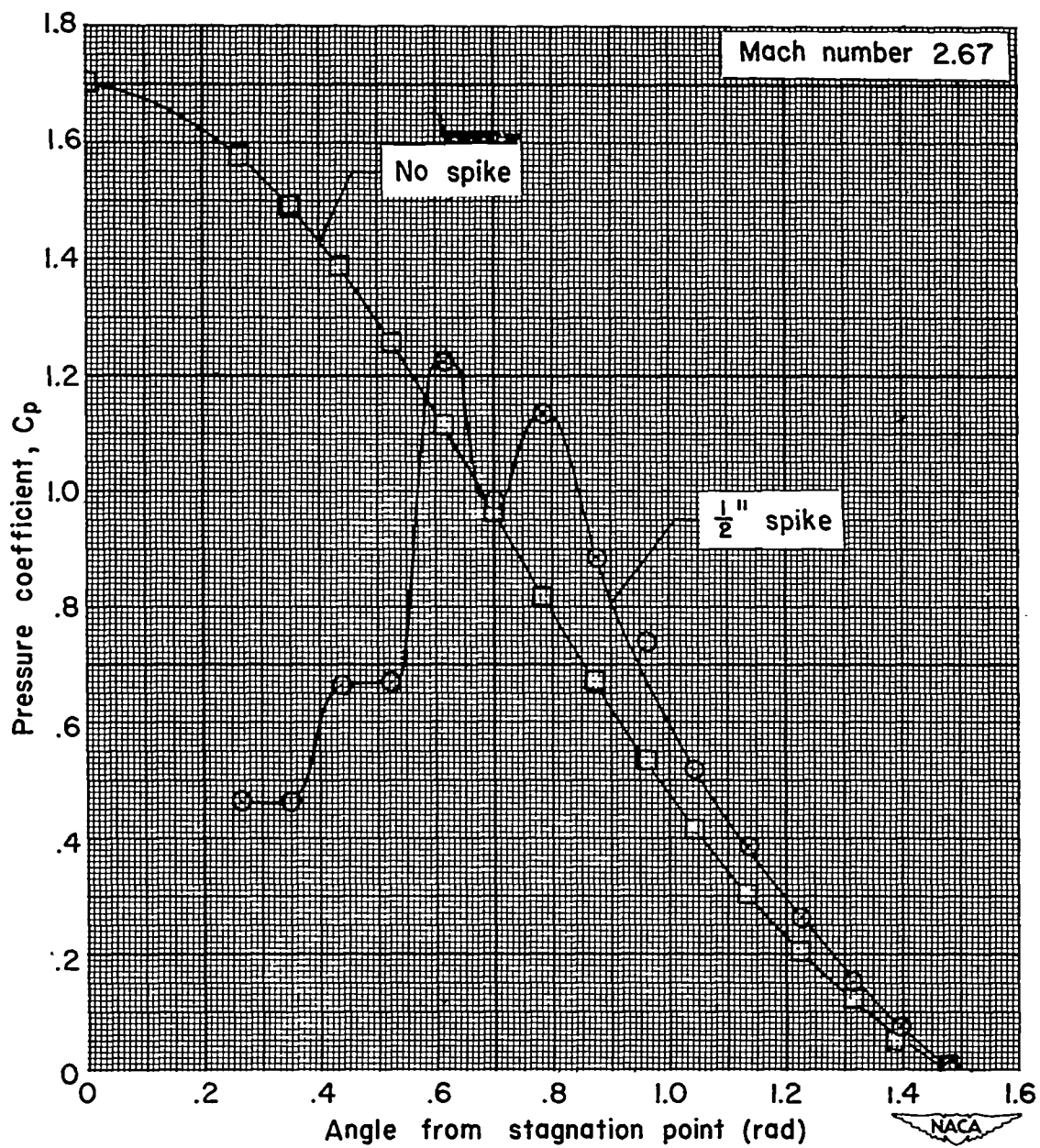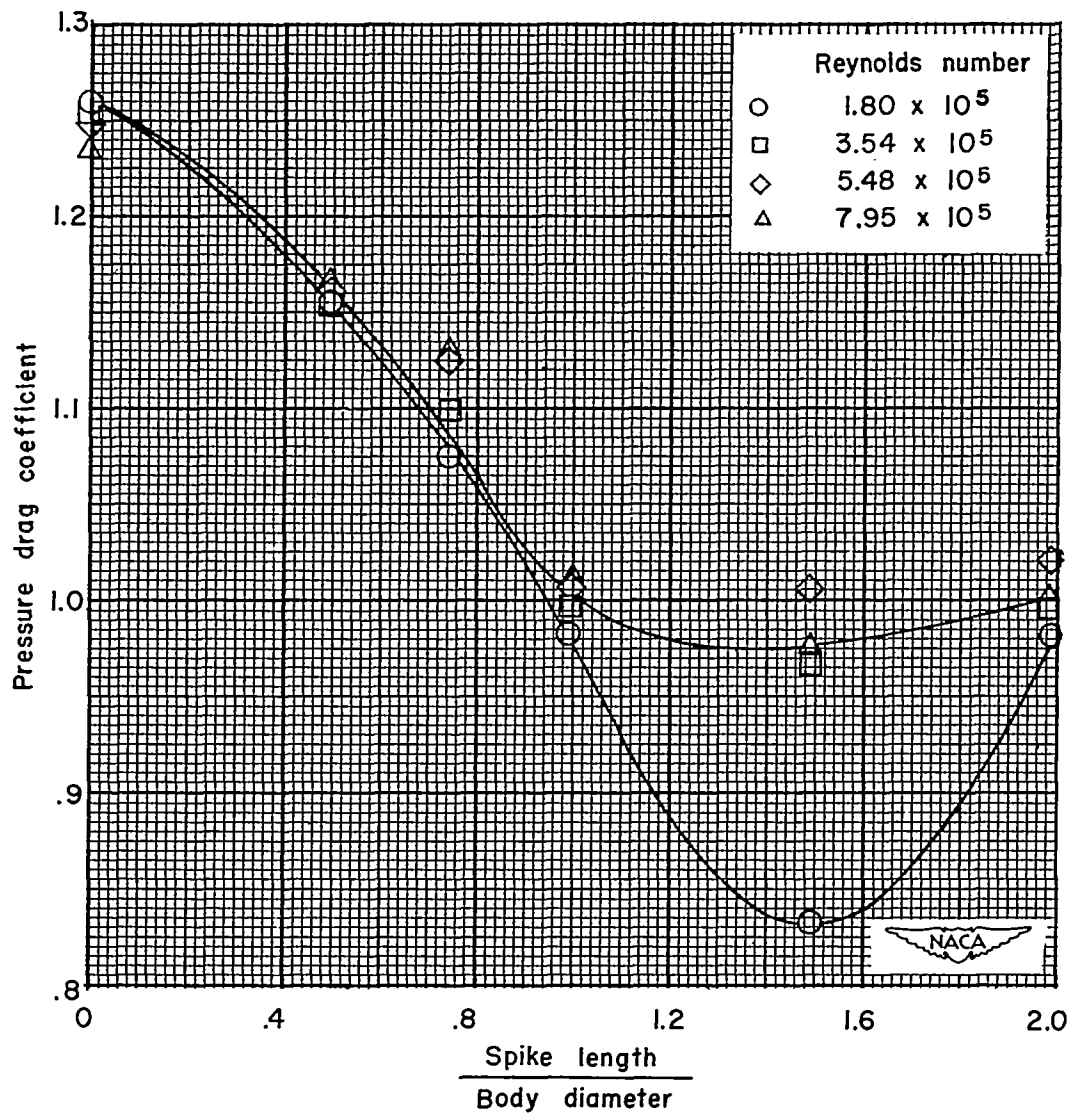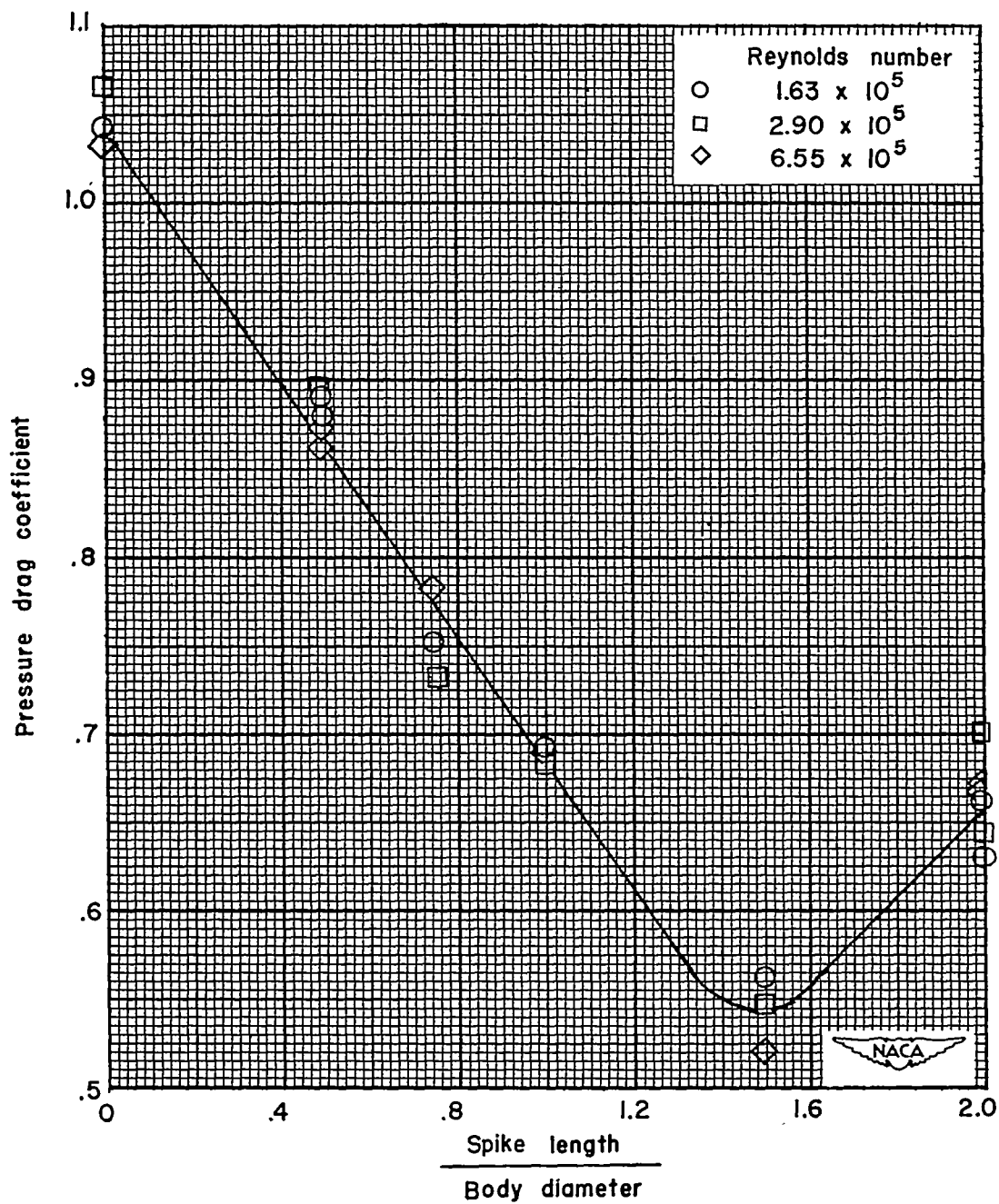of body; M = 2.67, $Re_D = 2.90 \times 10^5$.

Figure 12.- Typical pressure distribution about hemispherical nose of
model.

(a) M = 1.75

Figure 13.- Drag on hemispherical nose with spikes.

(b) M = 2.67

Figure 13.- Concluded.